RESILIENT INFRASTRUCTURE
June 1–4, 2016
RESILIENT INFRASTRUCTURE LONDON 2016

FLEXURAL BEHAVIOUR OF REINFORCED SCC BEAMS CONTAINING RECYCLED CRUMB RUBBER

Mohamed K. Ismail
Memorial University of Newfoundland, Canada

Assem A. A. Hassan
Memorial University of Newfoundland, Canada

Basem H. AbdelAleem
Memorial University of Newfoundland, Canada

ABSTRACT

This study aimed to investigate the effect of crumb rubber (CR) on the flexural behavior and cracking characteristics of self-consolidating concrete beams. Four full-scale self-consolidating rubberized concrete (SCRC) beams containing recycled CR particles as a partial replacement for fine aggregate with percentage ranging from 0% to 15% (by volume of sand) were tested. The performance of some design codes was evaluated in predicting the cracking moment and crack widths of the tested beams. The results indicated that increasing the CR content noticeably reduced the compressive strength, tensile strength, and first cracking moment of all SCRC beams. However, up to 15% replacement of CR, the flexural capacity of the tested beams was shown to be slightly decreased. In addition, increasing the CR content appeared to improve the beams' ductility and limit the flexural crack widths. In general, the results of flexural loading tests indicated a promising potential for using SCRC in structural applications.

Keywords: Self-consolidating concrete, crumb rubber, flexural strength, cracking behaviour.

1. INTRODUCTION

During the last years, discarded tires represent a large portion of solid wastes which have become a significant environmental concern, worldwide. Around 75% of these tires are burned or buried in landfills, while the remaining are used as raw materials to fuel factories (Eldin and Senouci, 1993). The United States found 2-3 billion scrap tires have accumulated in illegal remote areas including deserts and empty lots (Baoshan Huang and Guoqiang Li, 2004). There are many environmental and human health problems associated with the techniques that are commonly used to dispose of the worn-out tires, such as burning or piling up in landfills. Burning of waste tires releases toxic fumes that pollute the air (Garrick, 2005; Turer, 2012). Similarly, storing the wasted tires in landfills for a long time provides a suitable environment for insects and pests, which may lead to the spread of disease. (Mohammed et al., 2012; Wang et al., 2013; Thomas et al., 2015).

Many techniques have proposed to generate safe uses for scrap tires in construction industry. One of these techniques is the use of rubber particles as a partial replacement of fine or/and coarse aggregates in concrete. Significant research reported that although using waste rubber in concrete decreased its mechanical properties (Eldin and Senouci, 1993; Pelisser *et al.* 2011), the addition of rubber appeared to improve the fracture toughness, energy absorption, impact resistance, ductility, and reduced the density of concrete (Reda-Taha, 2008; Bharati Raj et al., 2011; Najim and Hall, 2014).

However, most of the available research focuses on investigating the behaviour of rubberized concrete mixtures using small-scale samples, but there is a dearth of data available regarding the structural behaviour of large-scale rubberized concrete elements, especially when self-consolidating rubberized concrete (SCRC) is used. The main objective of this research was to study the effect of crumb rubber (CR) on structural performance of full-scale

reinforced under flexural load. The investigation included evaluations of the effect of CR on the first crack load, flexural capacity, cracking characteristics, and curvature ductility of the tested beams.

2. EXPERIMENTAL PROGRAM

2.1 Materials Properties

Type GU Canadian Portland cement similar to ASTM C618 (2012) Type F was used as cementitious material for SCRC mixtures. Natural sand and 10 mm crushed stone aggregate were used as fine and coarse aggregates, respectively. Both aggregates have a specific gravity of 2.6 and absorption of 1%. A crumb rubber aggregates with a maximum aggregate size of 4.75 mm, a specific gravity of 0.95, and negligible absorption was used as a partial replacement of the fine aggregate in SCRC mixtures. Glenium 7700 high-range water-reducer admixture (HRWRA), similar to ASTM Type F (ASTM C494) (2013), was used to adjust the flow-ability and cohesiveness of SCRC mixtures. The tested beams contained two different bar diameters of 10 and 25 mm, as shown in Figure 1. All steel bars and stirrups had an average yield stress of 400 MPa.

2.2 Concrete Mixtures

The concrete mixtures in this investigation were selected based on a previous study by the authors (Ismail and Hassan 2015) aimed at developing a number of SCRC mixtures containing maximum percentages of CR (by volume of fine aggregate) and minimum reductions in strength and stability. In order to develop preliminary acceptable fresh properties for all tested SCRC mixtures, a trial mixtures stage was performed to determine the minimum water-to-binder (w/b) ratio and the minimum total binder content that can achieve acceptable SCRC flow-ability without overdosing the HRWRA. The results of the trial mixtures stage indicated that at least 0.4 w/b ratio and 500 kg/m^3 as a total binder content should be used to obtain SCRC having acceptable slump flow with no visual sign of segregation. Therefore, a w/b ratio of 0.4 and a minimum total binder content of 500 kg/m^3 were used in all tested mixtures (Table 1). Also, a constant coarse-to-fine aggregate (C/F) ratio of 0.7 was chosen for all tested mixtures. This ratio was chosen based on previous research (Hassan and Mayo 2014) carried out on SCC with different C/F aggregate ratios. The selected mixtures contained four SCRC mixtures with CR replacement of 0%–15%. All tested mixtures were designated by total binder content, and percentage of CR. For example, a beam containing a 500 kg/m^3 binder content, and 5% CR would be labelled as 500C-5CR.

Table 1: Mix Design for Tested Mixtures.

Beam #	Mixture	Cement (kg/m^3)	SCM (Type)	SCM (kg/m^3)	C. A. (kg/m^3)	F. A. (kg/m^3)	CR (kg/m^3)	HRWRA (kg/m^3)	Density (kg/m^3)
1	500C-0CR	500	-	-	686.5	980.8	0.0	2.37	2367.3
2	500C-5CR	500	-	-	686.5	931.7	17.9	2.37	2336.2
3	500C-10CR	500	-	-	686.5	882.7	35.8	2.37	2305.1
4	500C-15CR	500	-	-	686.5	833.7	53.8	2.37	2273.9

Note: All mixtures have a 0.4 w/b ratio; C. A. = Coarse aggregates; F. A. = Fine aggregates; CR = Crumb rubber.

2.3 Fresh and Hardened Concrete Property Tests

Slump flow diameter and time, and V-funnel and L-box tests were conducted to measure flow-ability, viscosity, and passing ability. These tests were conducted as per the European Guidelines for Self-Compacting Concrete (EFNARC 2005). The compressive strength and splitting tensile strength (STS) tests were conducted using 100 mm diameter x 200 mm height concrete cylinders, according to ASTM C39/C39M (2011) and C496/C496M (2011), respectively. The compressive strength and STS tests were implemented after the sample had been exposed to a curing condition similar to that of the tested beams. The results of the fresh and mechanical properties of the tested mixtures are presented in Table 2.

Table 2. Fresh and Mechanical Properties of Tested Mixtures.

Mixture #	Mixture	Slump flow		L-box H2/H1	V-funnel	Air %	28-Day f'_c	28-Day STS
		D_s mm	T_{50} sec		T_0 sec			
1	500C-	700	1.20	0.89	6.39	1.5	50.2	3.87
2	500C-	690	1.55	0.83	6.95	2.00	43.0	3.23
3	500C-	687	1.74	0.79	7.57	2.3	41.8	2.94
4	500C-	675	2.00	0.75	8.75	4.3	35.3	2.67

2.4 Casting of Beam Specimens, Flexural Test Setup, Instrumentation, and Loading Procedure

Four full-scale concrete beams were prepared using the 4 developed mixtures. Immediately after completing the fresh properties tests, the reinforced concrete beams were cast for each mixture. All SCRC beams were cast without consolidation; the concrete was poured from one side until it flowed and reached the other side. Formworks were removed after 24 hours of casting, and the beams were moist-cured for four days and then air-cured until the date of testing. All beams were designed to fail in flexure with a ductile behaviour. Figure 1 shows the beams' dimensions, reinforcement details, and test setup for all 4 concrete beams. A hydraulic jack with a capacity of 500-kN was used to apply a single-point loading onto a steel beam, which distributed the load into two-point loads acting on the beam surface. The mid-span deflection was measured using a linear variable differential transformer (LVDT) while two strain gauges were attached at the bottom of the longitudinal reinforcement to record the mid-span reinforcement strain. The beams were loaded gradually, with a constant loading rate through four stages until failure (first crack load, 50%, 75%, and 100% of the theoretically calculated failure load). After each stage of loading, the cracks were marked and their widths were recorded and plotted on each crack pattern. The overall behaviour of the beams, including the development of cracks, crack patterns, crack widths, crack heights, and failure modes, was observed and sketched for all beams (see Figure 2). The results obtained from the flexural testing of the 4 tested beams are presented in Tables 3 and 4.

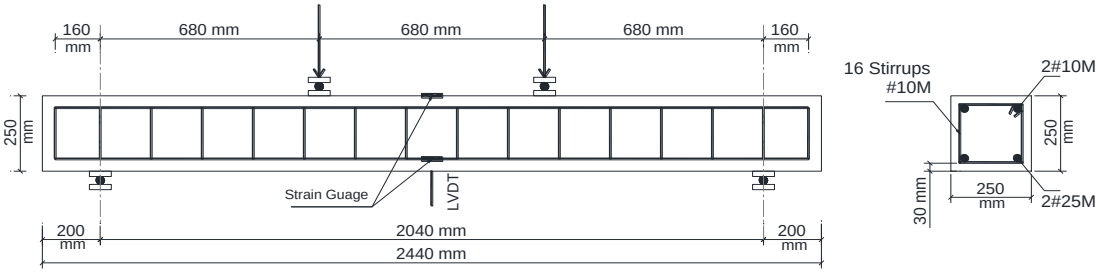

Figure 1: Beam dimensions, reinforcement details, and test setup.

Table 3: Results of Flexural Test of Tested Beams.

Beam #	Mixture	Deflection at ultimate load (mm)	Ultimate Flexural load (kN)	Experimental first cracking moment (kN.m)	Calculated cracking moment (kN.m)			
					ACI	CSA	AS	EC2
B1	500C-0CR	27.0	250.0	11.15	11.44	11.07	12.50	12.16
B2	500C-5CR	28.5	251.1	8.60	10.59	10.25	11.56	10.96
B3	500C-10CR	28.2	249.2	7.75	10.44	10.10	11.40	10.75
0B4	500C-15CR	30.8	243.3	7.28	9.59	9.28	10.48	9.60

Table 4: Cracking Characteristics of Tested Beams.

Beam #	Mixture	Number of cracks at different % of failure load			Experimental maximum crack width at different % of failure load				Calculated maximum crack width at different % of failure load (Gergely-Lutz Equation)				Calculated maximum crack width at different % of failure load (Frosch Equation)			
		50	75	100	First crack	50	75	100	First crack	50	75	100	First crack	50	75	100
B1	500C-0CR	8	11	16	0.035	0.24	0.60	5	0.060	0.38	0.62	1.78	0.035	0.22	0.36	1.03
B2	500C-5CR	11	13	18	0.028	0.22	0.56	4	0.064	0.43	0.68	1.96	0.037	0.25	0.39	1.13
B3	500C-10CR	11	13	17	0.026	0.20	0.48	3.5	0.047	0.44	0.67	1.24	0.027	0.25	0.39	0.71
B4	500C-15CR	13	15	19	0.023	0.19	0.46	3	0.047	0.45	0.74	1.44	0.027	0.26	0.43	0.83

3. DISCUSSION OF TEST RESULTS

3.1 Failure modes

The crack patterns of all tested beams indicated a typical flexural failure mode (See Figure 2). At early stage of loading, fine vertical flexural cracks were formed at the mid-span of all beams and the number of these cracks was increasing as the applied load increased. With further increase in load, new flexural cracks appeared in the shear spans and propagated diagonally due to the effect of flexural and shear stresses. At high stage of loading, the existing cracks grew wider forming small branches near their tips. Before failure, the steel reinforcement yielded first then the concrete crushed at the compression zone near the mid-span, indicating a ductile failure mode. Figure 2 shows the crack pattern of all tested beams at failure stage. The vertical and inclined lines in the figure represent the cracks formed along the loaded beams' span while the dark regions represent the concrete crushing zone. It should be noted that because adequate rebar's anchorage and shear reinforcement were provided, no bond or shear failure occurred in any of the tested beams.

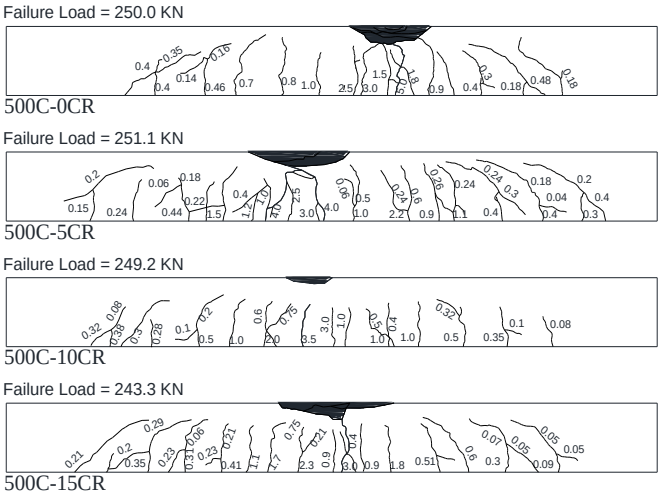

Figure 2: Crack patterns of tested beams at failure (crack width in mm)

3.2 Moment-Curvature Curve and Ductility

The moment-curvature of all tested beams are presented in Figure 3. It can be seen from the figure that the moment-curvature followed a typical pattern. Up to the first cracking moment, the curves appeared to be linear with high slopes. With further loading, the slope of the curves slightly reduced, showing a relatively higher rate of increase in the beams' curvature. At the rebar's yielding, the beams' curvature rapidly increased with a slight increase in the

moment. It should be noted that, the moment-curvature at the ultimate failure stage of the beam is not presented in Figure 3. This is because the top surface of the concrete beams cracked and crushed near the glued strain gauges at the ultimate failure stage which make it impossible to obtain reliable results from these gauges. For this reason, the relationships in Figure 3 were presented up to approximately 98% of the failure load and therefore, the ultimate curvature values were higher than the values reported herein.

.

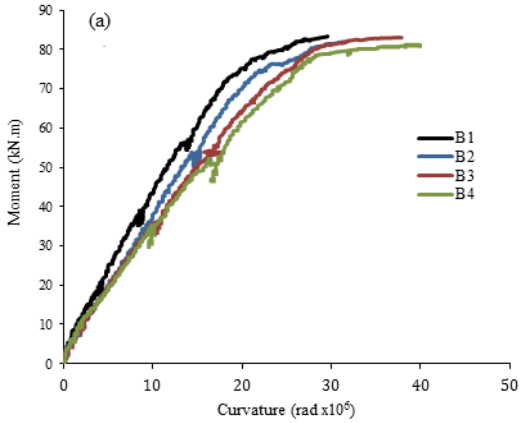

Figure 3: Moment-curvature curves of the tested beams

In the present work, curvature ductility factor (μ_ϕ) was used to evaluate the effect of CR on the deformability of the tested beams. Figure 4 shows the curvature ductility factor (μ_ϕ), which is expressed in term of $\mu_\phi = \phi_{98\%}/\phi_y$, where $\phi_{98\%}$ is the experimental curvature at 98% of ultimate failure load and ϕ_y is the curvature at the yield load. Generally, improving the ductility of structural member indicates increasing its ability to undergo large deformations prior to failure, thus providing early warning to the occupants before failure. While, increasing the percentage of CR from 0% to 15% showed an improvement in the ductility factor reached up to 25%. This result reflects the beneficial effect of inclusion CR particles in concrete, in which the low stiffness of rubber particles can contribute to enhancing the deformability and strain capacity of rubber-cement composite, and thus increasing the ductility of beams.

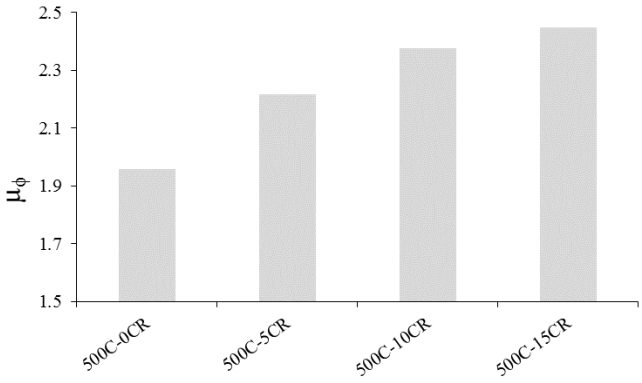

Figure 4. Curvature ductility of the tested beams.

3.3 Cracking Behaviour

Table 4 shows the experimental cracking characteristics (numbers and widths) of the tested beams at each loading stage. Figure 2 also shows the crack patterns of all tested beams at the failure stage. Based on the results, the inclusion of CR seemed to restrict the cracks from opening wider. The beam with no CR (B1) was found to exhibit wider crack widths compared to the rubberized concrete beams (B2–B4) at all stages of loading. However,

increasing the CR content raised beam's curvature, as shown in Figure 3, which led to a slight increase in the number of cracks.

In early ACI 318 provisions, the Gergely-Lutz equation (1973) (Eq. 1) was used to predict crack widths. In addition, the current Canadian code requires calculation of a crack width parameter based on the same equation. Eq. 1 was obtained by running a statistical analysis on crack width data from a number of investigations. The aim of this equation was to predict the maximum crack width at the surface of beams in areas of flexural tension. On the other hand, the new crack control calculations in ACI 318 (2008) rely on the Frosch's model (Eq. 2) (1999), which is adopted from fundamental crack control concepts presented by Broms (1965). Part of this investigation was to study the ability of the aforementioned equations (Eqs. 1 and 2) to predict the maximum crack widths at each stage of loading.

[1] $w = 11 \times 10^{-6} \beta f_s \sqrt[3]{d_c A} = 11 \times 10^{-6} \beta z$

Where $z = f_s (d_c A)^{1/3}$; w is the crack width in mm; β is the distance from the neutral axis to the bottom fibre divided by the distance to the centre of tensile reinforcement; f_s is the stress in the longitudinal reinforcement in MPa; d_c is the distance in mm from the extreme tension fibre to the centre of the reinforcing bar located closest to it; and A is the area of effective tension surrounding the tension reinforcement with the same centroid as the tension reinforcement, divided by the number of bars or wires in mm^2.

[2] $w = 2 \frac{f_s}{E_s} \beta \sqrt{d_c^2 + (\frac{s}{2})^2}$

where w is the crack width in mm; f_s is the stress in the longitudinal reinforcement in MPa; Es is the Young's Modulus of the longitudinal reinforcement in MPa; the value of β is approximately 1.0+0.0031dc (Frosch 2001), d_c is the distance from the extreme tension fibre to the centre of the reinforcing bar located closest to it in mm; s is the centre-to-centre spacing of tension reinforcement.

Table 4 compares the experimental and calculated (predicted) crack widths from Eqs. 1 and 2. As seen from the table for beams with/without CR, the calculated crack widths obtained by the Gergely-Lutz equation (up to 75% of the failure load) showed a comparatively high difference between the calculated crack widths and those obtained from the experiments. This can be attributed to the fact that the value of β is relatively high in shallow beams (β = 1.72), which heightened the prediction values. From Table 4, it can be also seen that increasing the percentage of CR led to heightening the difference between the expected values by Eq. 1 and that obtained from the experiments. Such observation may be related to that increasing the percentage of CR allowed higher number of cracks to be formed during loading, thus helping to reduce the overall cracking widths. However, at failure stage, the width of flexural cracks significantly increased, exceeding the calculated value. Adoption of the Gergely-Lutz equation by the Canadian code does not limit the crack width. However, it does limit the z-value in Eq. 1 to 30000 N/mm and to 25000 N/mm for interior and exterior exposure, respectively (CSA 2004). These limitations assume a constant value of 1.2 for β in order to limit the critical crack width to 0.40 for interior exposure and 0.33 mm for exterior exposure (CSA, 2004). For the tested beams with 250 mm depth, although the assumption of a constant value of β (= 1.2), as per CSA (2004), may yield lower values compared to those obtained from experiments, using the Gergely-Lutz equation generally over-predicted the maximum crack widths.

Using Frosch's model gave predicted values close to those measured from experiments, when applying up to 50% of the expected failure load (see Table 4). As the applied load increased to 75% and up to 100% of the failure load, the experimental crack widths significantly exceeded the calculated values. This could be related to the fact that up to 50% of failure load, the stress in the longitudinal reinforcement was below the yielding stress, while with further loading (75%–100% of the failure load) the stress exceeded the yielding limit, causing a larger widening in the flexural crack. The current ACI 318 adopted the Frosch's model without making a distinction between interior and exterior exposure. It requires that for crack control in beams the spacing of reinforcement closest to a surface in tension shall not exceed a limiting value calculated based on concrete cover and stress level in tensile reinforcement bars, in which the maximum spacing for tensile reinforcement is 300 mm. For the case of the tested beams with 30 mm clear cover, to limit the crack width to 0.4 mm at stress in longitudinal reinforcement equal to $0.6f_y$ (at service

load), the maximum required spacing should be 282 mm, which is higher than that used in all tested beams (145 mm).

From the perspective of serviceability, to fix problems with long-term durability most design codes limit the maximum allowable crack width at service load based on exposure condition. Focusing on 40% of the failure load, which can represent the customary level service load (Gholamreza et al. 2009), it can be observed that the maximum crack width of the tested beams up to 50% of the failure load (as shown in Table 4) did not exceed the critical crack width for the exterior exposure condition given by CSA-04 (0.33 mm), ACI 318-95 (0.33 mm), and BS 8110-97 (0.3 mm). Also, the results from up to 50% of the failure load met the limit of 0.3 mm maximum crack width tabulated by ACI 224R (2001) and CEB-FIP (1990) with respect to specific requirements such as water tightness or specific exposure classes. This finding indicates a potential applicability for using rubberized concrete safely in exterior-exposed structures.

3.4 Ultimate Flexural Capacity and Cracking Moment

Table 3 presents the ultimate failure load and cracking moment (M_{cr}) values of all tested beams. The results showed that increasing the CR content generally reduced the ultimate flexural capacity and cracking moment of the tested beams. Varying the percentage of CR from 0% to 15% CR slightly decreased the ultimate flexural load by 2.67%, while the first cracking moment showed a significant reduction reached up to 34.76%. The significant reduction in the load associated with the first flexural crack could be related to the significant decay in the tensile strength of the concrete when the CR content increased, as shown in the STS test results (Table 2).
In this part of the investigation, a comparison between the experimental and theoretical cracking moment ($M_{cr}^{pred.}$) was conducted. The theoretical values of $M_{cr}^{pred.}$ were calculated based on various codes as follows:

As per ACI-318 (2008):

[3] $$M_{cr} = f_r \frac{I_g}{y_t}$$

where $f_r = 0.62\lambda \sqrt{f_c'}$ for normal-weight concrete; λ is taken as equal to 1 for normal-density concrete and 0.85 for semi-low-density concrete; y_t is the distance from centroid axis of the gross section to the extreme tension fiber; and Ig is the second moment of area of the gross section (the steel bars are not considered).

As per CSA (2004):

[4] $$M_{cr} = f_r \frac{I_g}{y_t}$$

Where $f_r = 0.6\lambda \sqrt{f_c'}$ for normal-weight concrete; λ is taken as equal to 1 for normal-density concrete and 0.85 for semi-low-density concrete; y_t is the distance from centroid axis of the gross section to the extreme tension fiber; and I_g is the second moment of area of the gross section (the steel bars are not considered).

As per the Australian Standard (AS 3600 1988):

[5] $$M_{cr} = Z f_{cf}'$$

where f_{cf}' is the characteristic flexural tensile strength of the concrete = $0.6 \sqrt{f_c'}$; and Z is the section modulus of the uncracked section, referring to the extreme fiber at which cracking occurs.

As per Eurocode (EC2 2004):

[6] $$M_{cr} = f_{ctm} \frac{I_u}{(h - x_u)}$$

where f_{ctm} is the mean value of axial tensile strength of concrete = $0.3f_{ck}^{0.67}$; f_{ck} is the characteristic compressive cylinder strength of the concrete at 28 days; I_u is the second moment of area of the uncracked section; x_u is the distance from the neutral axis of the section to the extreme top fiber; and h is the height of the cross section of the beam. The characteristic strength of concrete (f_{ck} and f_{cf}) is defined as the value of concrete strength, which is exceeded by 95% of the control specimens.

Eqs. 3–6 were used to calculate the $M_{cr}^{pred.}$, and hence the first cracking load of the experimental beams. Table 3 and Figure 5 show the value of $M_{cr}^{pred.}$ calculated by ACI, CSA, AS, and EC2 compared to the experimental cracking moment ($M_{cr}^{exp.}$) of the tested beams. The results showed that increasing the CR content generally exhibited higher predicted values compared to those obtained from experiments. This could be attributed to the fact that the inclusion of CR had weakened the concrete mixtures because of the formation of a weak interfacial transition zone (ITZ) around the CR. Since the tensile strength is more critical to the strength of the ITZ, adding more CR showed lower $M_{cr}^{exp.}$ and thus increased the error of codes' prediction. The tensile strength in the design code equations is not taken from the experiments but rather predicted based on the compressive strength of concrete. For example, ACI and CSA assumed the tensile strength as a proportion from the square root of the compressive strength of concrete (tensile strength = $0.6\sqrt{f_c'}$), while EC2 derived the tensile strength using another relationship (tensile strength = $0.3f_{ck}^{0.67}$). Therefore, the design code equations used for predicting the first cracking moment may need to be reconstructed to be compatible with the performance of rubberized concrete beams. However, the above results are still based on limited tested mixtures. Therefore, it is recommended that additional experimental investigation be conducted to evaluate the applicability of the design code equations for predicting the first cracking moment of beams containing CR. From Figure 5, it can also be noticed that both ACI and CSA predictions gave lower values compared to AS and EC2. The ratio of $M_{cr}^{pred.}$/ $M_{cr}^{exp.}$ ranged from 1.03 to 1.49 in ACI and from 0.99 to 1.45 in CSA, while AS and EC2 had ratios that varied from 1.12 to 1.92 and from 1.09 to 1.67, respectively. This difference can be attributed to the fact that ACI and CSA codes neglect the effect of longitudinal reinforcement, while AS and EC2 take it into account in the calculation of the second moment of area of the uncracked section, yielding higher predicted values.

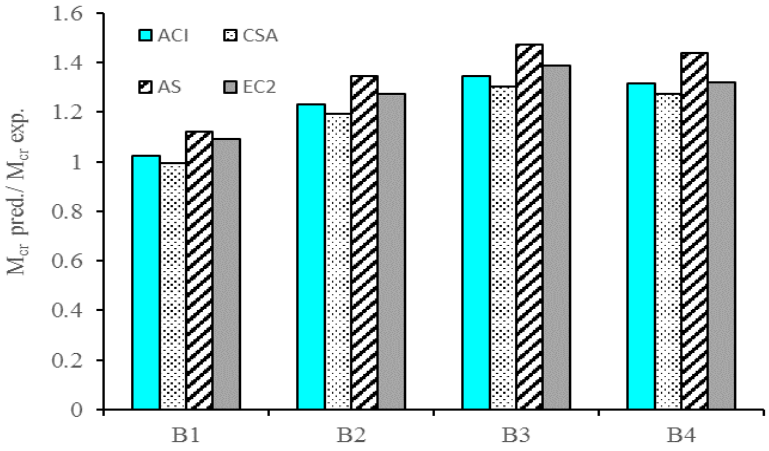

Figure 5: Code design performance in predicting the first cracking moment.

4. CONCLUSIONS

The following conclusions can be drawn from the results of this study:

1. Inclusion of 15% CR in SCRC mixtures showed a reduction in the compressive and tensile strengths reached up to 29.7% and 31%, respectively.
2. The reduction in the tensile strength of rubberized concrete due to the formation of a weak mortar-rubber interface showed a considerable reduction in the first cracking moment of the tested beams reached up to 34.7%, when 15% CR was used. Meanwhile, the flexural capacity showed a slight reduction of 2.67%.

3. As the percentage of CR increased, the deformation capacity and ductility of the tested beams appeared to be improved. For example, increasing the percentage of CR from 0% to 15% showed an improvement in the ductility factor reached up to 25%.
4. The Frosch's model predicted the crack width reasonably up to 50% of the failure load for SCRC beams, but significantly underestimated the crack widths at 75% and 100% of the failure load when the longitudinal steel reinforcement yielded. On the other hand, the Gergely-Lutz equation showed overpredicted values up to 75% of failure load due to the higher β-value in shallow beams.
5. According to the limitations of crack width given by the design codes considered in this study (CSA A23.3-04, ACI 318-95, BS 8110-97, ACI 224R-01, and CEB-FIP MC90) at service load level (40% of failure load), the results of the tested beams indicated a potential applicability for using rubberized concrete safely in exterior-exposed structures.
6. For beams with no CR (CR = 0%), all the investigated code-based equations (ACI, CSA, AS, and EC2) reasonably predicted the first cracking moment compared to that obtained from experiments. Increasing the CR content, however, showed a significant reduction in the experimental first cracking moment compared to the predicted values in all tested code-based equations.

ACKNOWLEDGEMENT

The authors would like to acknowledge the Research & Development Corporation of Newfoundland and Labrador (RDC) for sponsoring this work as part of a larger research project**.**

REFERENCES

ACI Committee 224. (2001). Control of Cracking in Concrete Structures (224R-90). American Concrete Institute, Farmington Hills, Mich., 43 pp.5.

ACI Committee 318. (1995). Building Code Requirements for Structural Concrete (ACI 318-95) and Commentary (ACI 318R-95). American Concrete Institute, Farmington Hills, MI, 465 pp.

ACI Committee 318. (2008). Building Code Requirements for Structural Concrete (ACI 318) and Commentary (ACI 318R-08). American Concrete Institute, Farmington Hills, MI, 465 pp.

AS 3600. (1988). Concrete Structures. Standards Association of Australia, Sydney, Australia.

ASTM C39/C39M-14. (2011). Standard test method for compressive strength of cylindrical concrete specimens. *ASTM International*, West Conshohocken, PA, USA.

ASTM C494/C494M-13. (2013). Standard Specification for Chemical Admixtures for Concrete. *ASTM International*, West Conshohocken, PA, USA.

ASTM C496. (2011). Standard Test Method for Splitting Tensile Strength of Cylindrical Concrete Specimens. *ASTM International*, West Conshohocken, PA, USA.

ASTM C618. (2012). Standard Specification for Coal Fly Ash and Raw or Calcined Natural Pozzolan for Use in Concrete. *ASTM International*, West Conshohocken, PA, USA.

Baoshan H. (2004). Investigation into Waste Tire Rubber-Filled Concrete. *Journal of Materials in Civil Engineering, ASCE,16(3):187-194.*

Bharati R. (2011). Engineering properties of self-compacting rubberized concrete. Journal of Reinforced Plastics and Composites, 30(23): 1923-1930

Biel, T. D., and Lee, H. (1994). 'Use of recycled tire rubbers in concrete. Proc., ASCE 3rd Mat. Engrg. Conf., Infrastructure: New Mat. and Methods of Repair, 351–358.

British Standard Institute. (1997). Structural Use of Concrete-Part 1: Code of Practice for Design and Construction.

Broms, B. B. (1965). Crack Width and Crack Spacing in Reinforced Concrete Members. *ACI Journal,* 62(10), 1237-1256.

Canadian Standards Association Committee A23.3. (2004). Design of Concrete Structures. *CSA A23.3-04, Canadian Standards Association*, Rexdale, Ontario.

CEB-FIP. (1992). CEB-FIP Model Code 1990. Thomas Telford, London.

EFNARC. (2005). The European Guidelines for Self-Compacting Concrete Specification, Production and Use. English ed. Norfolk, UK: European Federation for Specialist Construction Chemicals and Concrete Systems.

EN 1992-1-1. (2004). Eurocode 2 – Design of Concrete Structures – Part 1–1: General rules and rules for buildings. Thomas Telford, London, UK.

Eldin, N. N. and Senouci, A. B. (1993). Rubber-Tire Particles as Concrete Aggregate. *Journal of Materials in Civil Engineering, ASCE*, 5(4): 478–496.

Frosch, R. J. (1999). Another Look at Cracking and Crack Control in Reinforced Concrete. *ACI Structural Journal*, 437 – 442.

Frosch, R. J. (2001). Flexural Crack Control in Reinforced Concrete. Design and Construction Practices to Mitigate Cracking, SP 204, American Concrete Institute, Farmington Hills, Mich., 135-154.

Ganesan, N., Bharati, R. J. and Shashikala, A. P. (2013). Behavior of Self-Consolidating Rubberized Concrete Beam-Column Joints. ACI Materials Journal, 110, 697-704.

Garrick, G. (2005). Analysis and testing of waste tire fiber modified concrete. Master thesis. The Department of Mechanical Engineering, the Graduate Faculty of the Louisiana State University and Agricultural and Mechanical College. cookie

Gergely, P. and Lutz, L. A. (1973). Maximum Crack Width in Reinforced Concrete Flexural Member. *ACI SP-20*, Detroit, 87-117.

Gholamreza, F. A. G., Razaqpur, O. B. I., Abdelgadir, A., Benoit, F. and Simon, F. (2009). Flexural Performance of Steel-Reinforced Recycled Concrete Beams. *ACI Structural Journal,* 106 (6): 858-867.

Hassan, A. A. A. and Mayo, J. R. (2014). Influence of Mixture Composition on the Properties of SCC Incorporating Metakaolin. *Magazine of Concrete Research*, 66(1): 1–15.

Ismail, M. K. and Hassan, A. A. A. (2015). Influence of Mixture Composition and Type of Cementitious Materials on Enhancing the Fresh Properties and Stability of Self-Consolidating Rubberized Concrete. *Journal of Materials in Civil Engineering*. http://ascelibrary.org/doi/abs/10.1061/(ASCE)MT.1943-5533.0001338.

Mohammed, B. S., Khandaker, M., Anwar, H., Jackson, T. E. S., Grace, W. and Abdullahi, M. (2012). Properties of crumb rubber hollow concrete block. Journal of Cleaner Production 23: 57-67.

Najim, K. B. and Hall, M. (2014). Structural Behaviour and Durability of Steel-Reinforced Structural Plain/Self-Compacting Rubberised Concrete (PRC/SCRC). *Construction and Building Materials*, 73, 490–497

Pelisser, F., Zavarise, N., Longo, T. A. and Bernardin, A. M. (2011). Concrete Made with Recycled Tire Rubber: Effect of Alkaline Activation and Silica Fume Addition. *Journal of Cleaner Production*, 19(6): 757–763.

Taha, M. M. R., El-Dieb, A. S., Abdel-Wahab, M. A. and Abdel-Hameed, M. E. (2008). Mechanical, Fracture, and Microstructural Investigations of Rubber Concrete. *Journal of Materials in Civil Engineering*, ASCE, 20, 640–649.

Thomas, B. S., Gupta, R. C., Mehra, P. and Kumar S. (2015). Performance of high strength rubberized concrete in aggressive environment. *Construction and Building Materials* 83: 320-326.

Turer, A. (2012). Recycling of scrap tires. Material Recycling- Trends and Perspectives, pp. 195-212.

Wang H. Y., Yung L. C. and Hua L. H. (2013). A study of the durability properties of waste tire rubber applied to self-compacting concrete. *Construction and Building Materials* 41: 665-672.